J. Fluid Mech. (1987), *vol.* 178, *pp.* 405–421
Printed in Great Britain

The wave structure of turbulent spots in plane Poiseuille flow

By DAN S. HENNINGSON† AND P. HENRIK ALFREDSSON
Department of Mechanics, The Royal Institute of Technology, S-100 44 Stockholm, Sweden

(Received 18 January 1986 and in revised form 14 October 1986)

The wave packets located at the wingtips of turbulent spots in plane Poiseuille flow have been investigated by hot-film anemometry. The streamwise velocity disturbances associated with the waves were found to be antisymmetric with respect to the channel centreline. The amplitude of the waves had a maximum close to the wall that was about 4 % of the centreline velocity. The modified velocity field outside the spot was measured and linear stability analysis of the measured velocity profiles showed that the flow field was less stable than the undisturbed flow. The phase velocity and amplitude distribution of the waves were in reasonable agreement with the theory, which together with the symmetry properties indicate that the wave packet consisted of the locally least stable Tollmien–Schlichting mode.

1. Introduction

If a wave-like disturbance is introduced by a vibrating ribbon into a laminar boundary layer (Klebanoff, Tidstrom & Sargent 1961) or Poiseuille flow (Nishioka, Iida & Ichikawa 1975) the linear hydrodynamic stability theory is able to predict whether the resulting Tollmien–Schlichting (T–S) waves are amplified or not. For Poiseuille flow the linear theory gives the critical Reynolds number (*Re*), i.e. the Reynolds number below which no wave disturbance is amplified, as 5772 (based on centreline velocity and channel half-height) (Orszag 1971). Nishioka *et al.* found that the linear theory was valid until the amplitude of the waves reached a few percent of the centreline velocity. Then the growth rate became higher than the exponential growth predicted by the theory. Hence it seems that when the amplitude reaches this level nonlinear effects start to become important.

The vibrating-ribbon experiments confirm the applicability of the linear stability theory, however, growth of two-dimensional waves is not the only route to transition. Gaster & Grant (1975) introduced a point-like disturbance into a laminar boundary layer and found that it gave rise to a bow-shaped wave packet, which grew in size and amplitude as it travelled downstream. Gaster (1975) was able to model the wave packet development by calculating the spatial growth rates for the least stable mode of an initial disturbance with a flat spectrum. The wave packet was then calculated as a linear combination of all wavenumbers, and excellent agreement between experiments and calculations was obtained. It was possible to follow the disturbance over more than one hundred boundary-layer thicknesses before signs of nonlinear effects began to appear in the experiments. These would ultimately lead to breakdown and generation of a turbulent spot.

Experimentally one finds that if the amplitude of the point disturbance and the

---

† Present address: The Aeronautical Research Institute of Sweden, s-16111 Bromma, Sweden.

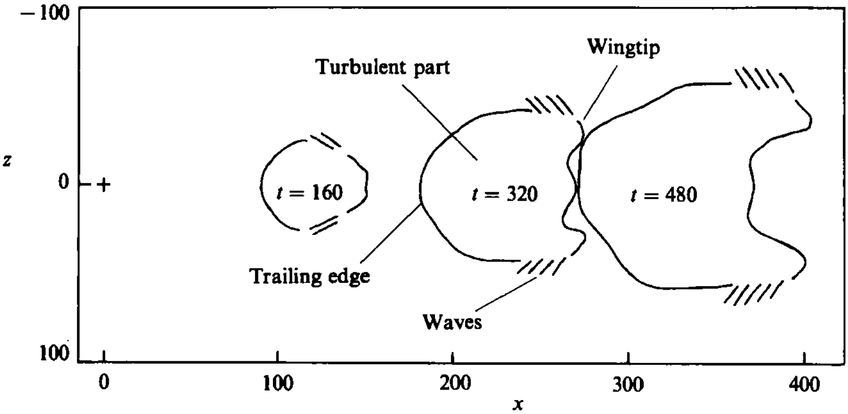

FIGURE 1. Development of a turbulent spot in plane Poiseuille flow, $Re = 1600$. The full lines indicate the edges of the turbulent regions. +, spot triggering position.

Reynolds number of the flow are high enough a turbulent spot may develop without the intermediate steps of wave formation and growth. For plane Poiseuille flow on the one hand turbulent spots may be triggered and sustained even at $Re = 1000$ (Carlson, Widnall & Peeters 1982; Alavyoon, Henningson & Alfredsson 1986), i.e. at a Reynolds number six times lower than the critical Reynolds number obtained from the linear stability theory. In boundary layers, on the other hand, spots are not usually obtained until well above the critical Reynolds number (see e.g. Wygnanski, Haritonidis & Kaplan 1979).

Both in boundary layers and plane Poiseuille flow one finds wave packets in conjunction with turbulent spots. Wygnanski *et al.* (1979) discovered wave packets upstream of the 'wingtips' of the spot, one on each side of the spot symmetry line. These wave packets moved with a lower celerity than the trailing edge of the spot and thus became detached from the spot. They found that the wave packets had much in common with the outer parts of the wave disturbance studied by Gaster & Grant (1975). Chambers & Thomas (1983), using flow visualization, concluded that the initial disturbance gives rise both to a turbulent spot and a wave packet and that these, due to their different celerities, are separated and become independent of each other.

The development of the wave packet in plane Poiseuille flow is quite different, however. Flow visualizations (Carlson *et al.* 1982; Alavyoon *et al.* 1986) have shown that the wave packet is attached to the 'wingtips' of the spot and follows the spot as it moves downstream (see figure 1, unpublished data from the study of Alavyoon *et al.* 1986). It has been hypothesized that the wave packets consist of T–S waves although such waves should be damped at the Reynolds number of these experiments ($Re = 1000$–2500). However, as the spot moves slower than the surrounding background flow it acts as a blockage (Widnall 1984) and the laminar flow field outside the spot will be altered. This may change the stability properties of that region. If the wave disturbance is amplified it may break down and thereby be responsible for the spreading of the spot.

The main motive of this study was to investigate the wave packets observed at the wingtips of turbulent spots in plane Poiseuille flow. Both the wave packet structure itself and the alteration of the velocity field outside the spot were studied. This was complemented by linear stability analysis of the measured velocity field.

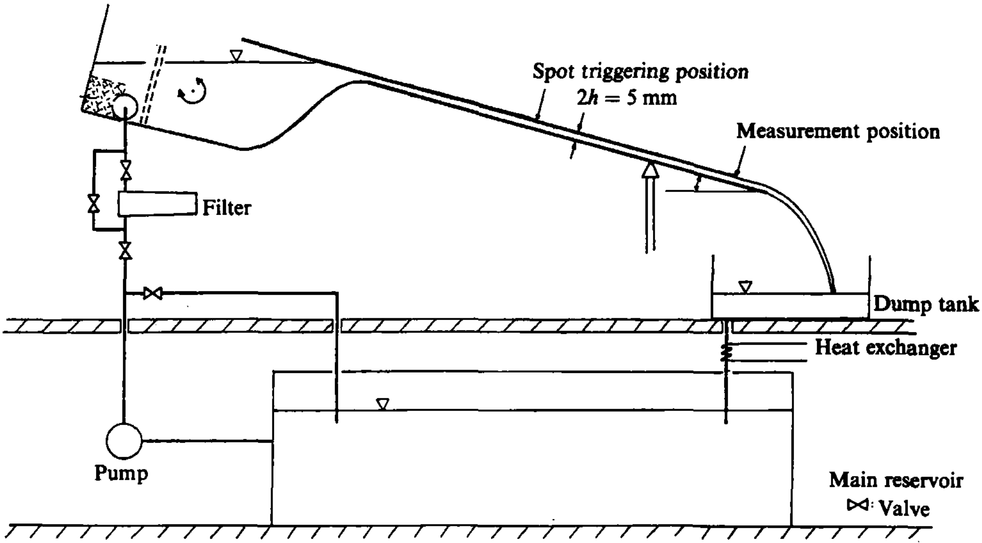

FIGURE 2. Experimental apparatus. Spot triggering position was 0.4 and 1.0 m from the measurement position.

The results predicted from the analysis were fairly close to the measured wave properties and it was also found that the region outside the spot was less stable than the undisturbed flow.

2. Experimental apparatus and technique

The apparatus was that used by Alavyoon *et al.* (1986) and is shown in figure 2. The channel section consists of two parallel flat glass plates and was 2 m long × 0.83 m wide. The channel height could easily be varied by using spacers of different dimensions, although all results presented in this study were taken with a channel height ($2h$) of 5 mm. The height was checked with a microscope technique (for a description see Alavyoon *et al.*) and was found to be constant within $\pm 3\%$. The main part of the measurements was carried out at a Reynolds number of 1500, corresponding to a centreline velocity of about 0.60 m/s. The spots were triggered by a solenoid which produced a jet of water of small diameter and duration, which entered the channel from the upper wall. Two positions were used for the triggering, namely 0.4 and 1.0 m from the downstream end of the channel. At the measurement position this corresponds to $x/h = 160$ and 400, respectively. (x and z are the coordinates in the streamwise and spanwise directions, respectively: $x = 0$ is at the triggering point and $z = 0$ is at the spot symmetry line, y is the coordinate normal to the walls, with $y = 0$ at the channel centreline. In the following all quantities are made non-dimensional in the appropriate way with the channel half-height (h) and the undisturbed centreline velocity (U_{CL}).)

The velocity measurements were carried out with hot-film probes (DISA R15 and TSI 1261-10W) using the DISA 55M01 anemometers. The probes could be calibrated in a submerged water jet and were positioned in the flow from the end of the channel, i.e. they intruded only a few mm into the channel. We believe that end effects were small, which is substantiated by the fact that the measured velocity profiles were very close to the expected parabolic one. All data sampling and evaluation was carried out with a DEC MINC-system (PDP11/23). The solenoid was activated manually and at the same time the data acquisition was started through the Schmitt-trigger of the MINC-system.

To measure the spanwise velocity component the probe was positioned so that the normal of the sensor was at an angle ψ to the streamwise direction. Then the effective cooling velocity sensed by the hot-film becomes

$$U^2_{\text{cool}}/\cos^2\psi = (U_{\text{p}}+u+w\tan\psi)^2+\eta^2(w-(U_{\text{p}}+u)\tan\psi)^2,$$

where η is the tangential cooling coefficient and u and w are corrections to the mean parabolic profile, $U_{\text{p}}(y)$. By calibrating the probe *in situ* with the same angle as in the measurement, the tangential-cooling correction term resulting from the U_{p} velocity (i.e. $\eta^2U_{\text{p}}^2\tan^2\psi$) is automatically taken into account. What remains after a Taylor expansion is an expression of the form:

$$U_{\text{meas}} = (U_{\text{p}}+u+w\tan\psi)\left(1+\eta^2O\left(\frac{w}{U_{\text{p}}}\right)\right). \tag{1}$$

For ψ around 45° the DISA probe has $\eta \approx 0.35$. The deviations u and w are typically about 10 % of the mean velocity. Thus the error in (1) is a few percent. If u is determined from measurements with $\psi = 0$ then w may be calculated from (1).

3. Experimental results

3.1. *Spot spreading angle*

In this study the contraction section was slightly modified as compared to that of Alavyoon *et al.* (1986). This led to an increase in the Reynolds number (from 2200 to 3100) for which spontaneous transition occurred. Some results for the spot spreading half-angle (ϕ) obtained from flow visualization have been reported earlier. In this study another approach to determine the spreading angle was adopted. A hot-film probe was located at the downstream end of the channel at the spanwise position where about one out of ten spots gave rise to a turbulent signal. This position was then used to calculate the spreading angle (figure 3). The results agree fairly well with the data of Alavyoon *et al.*, although if there is a change in the virtual origin with Reynolds number, this is not taken into account in the present method. For the largest spreading angles there may be some effects of the channel sidewalls since the spot covered about 60 % of the channel width.

3.2. *Wave structure*

Figure 4 shows typical streamwise velocity signals at 7 different y-positions at $x = 400$ and $z = 62$, i.e. about two channel heights outside the turbulent part of the spot. The Reynolds number here and in all following measurements was 1500. The wave amplitude was largest, almost 4 % of the centreline velocity, at $y = 0.7$. At $y = 0.4$ waves were occasionally found, whereas no waves were found in the region $y < 0.4$. A feature in common for all y-positions was an increase in the velocity in the region of the wave packet. The same feature was found also at $x = 160$. From these two measurements the propagation velocity of the region of excess velocity was found to be about 0.75.

To separate the wave disturbance from the change in velocity, digital filtering using fast Fourier transform (FFT) routines was used. First the forward FFT was carried out: then inverse transforms were performed separately on the parts of the frequency-domain signal above a certain frequency (to obtain the waves) and below (to obtain

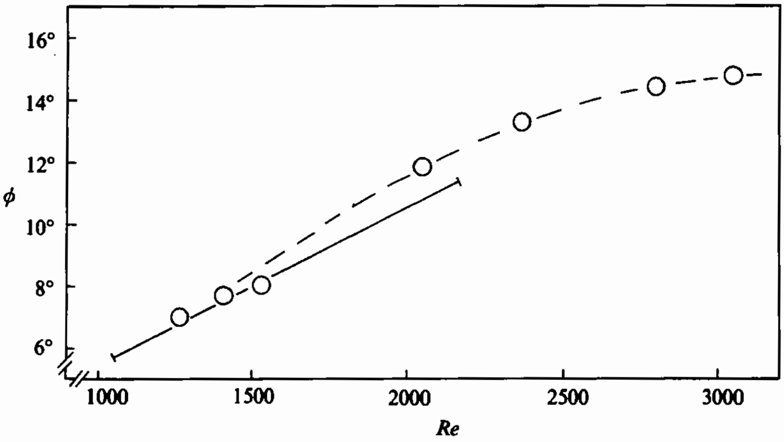

FIGURE 3. Spreading half-angle of spot *vs*. *Re*. ○, present results; ——, best-fit line to data of Alavyoon *et al*. (1986).

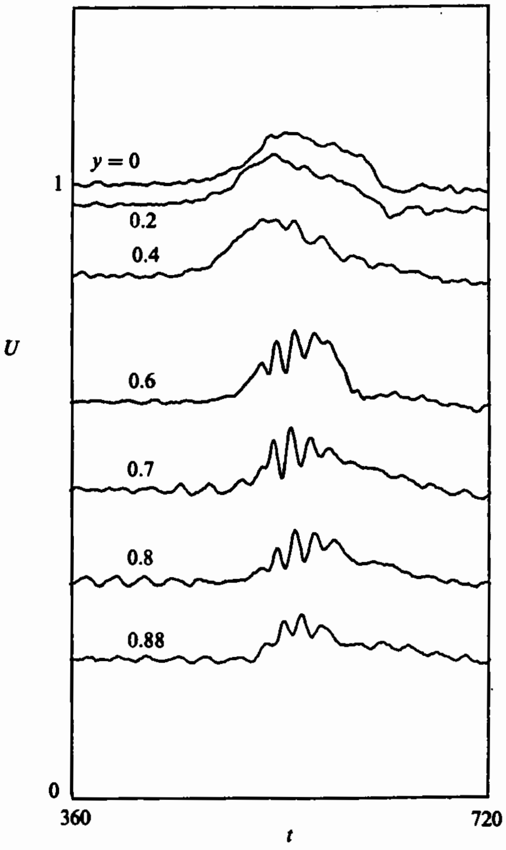

FIGURE 4. Velocity signals at seven different heights outside the wingtip of the spot. $x = 400, z = 62$. $t = 0$ is at the triggering time.

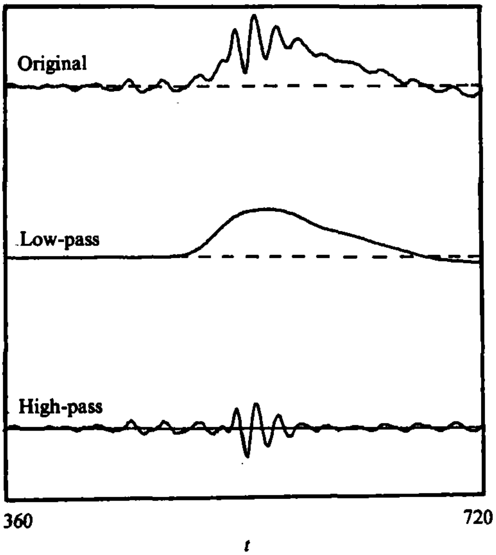

FIGURE 5. Original, low-pass- and high-pass-filtered velocity signals at $y = 0.7$. The Fourier coefficients have been set equal to zero above, and below $\omega = 0.16$ respectively.

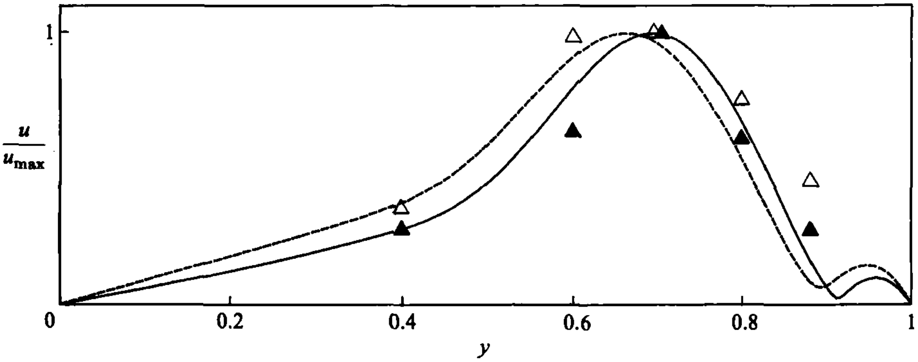

FIGURE 6. Amplitude dependence of the streamwise velocity disturbance obtained from two independent measurement series. $x = 400, z = 62$. △, ▲, experiment; ----, ——, theory according to §4.

the change in velocity). The choice of this filter frequency was not critical. Figure 5 shows a typical example.

The wave-amplitude distribution in the streamwise direction was determined by ensemble averaging the high-pass-filtered velocity signals of ten spot passages at each wall distance. Ten spots were judged to be sufficient since the flow was laminar and the repeatability good. However, if the spot triggering time was used as reference time for the averaging, too much phase jitter resulted. The approach adopted was to determine the highest wave peak and use this maximum as a reference for the ensemble averages. The two minima around the maximum of the ensemble average were used to evaluate the wave amplitude. Figure 6 shows the results at $x = 400, z = 62$ from two independent measurement series. It is worth noting that the velocity disturbance associated with the wave packet was about 30 % smaller

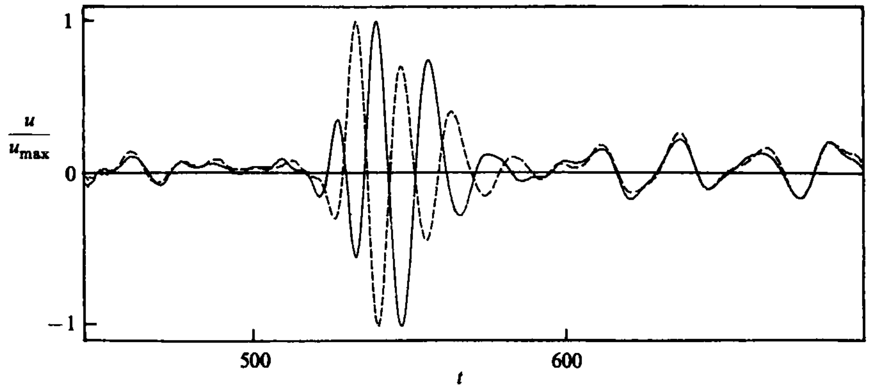

FIGURE 7. High-pass-filtered velocity signals from two probes, showing the antisymmetric property of the u-disturbance. $x = 400, z = 62$. ——, $y = -0.7$; ----, $y = 0.7$.

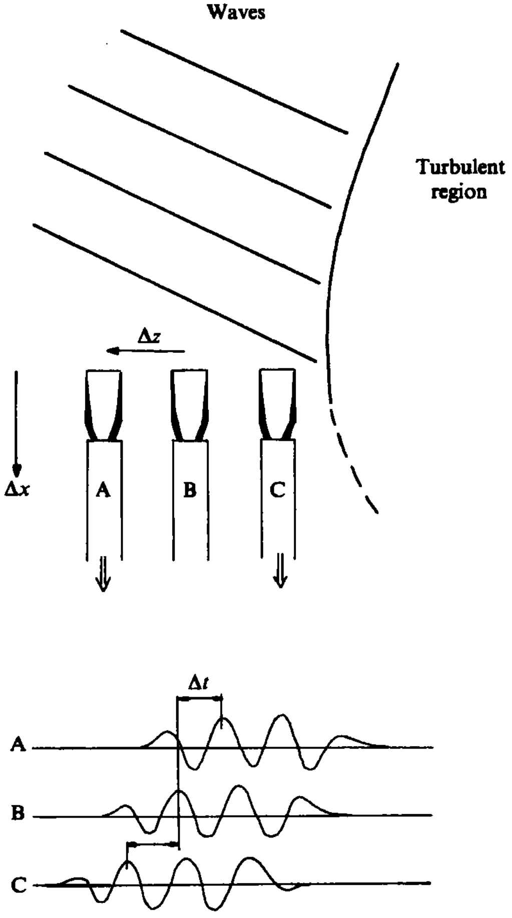

FIGURE 8. Probe configuration for measurements of wave properties. The reference probe is at position B, whereas the movable probe is at position A or C.

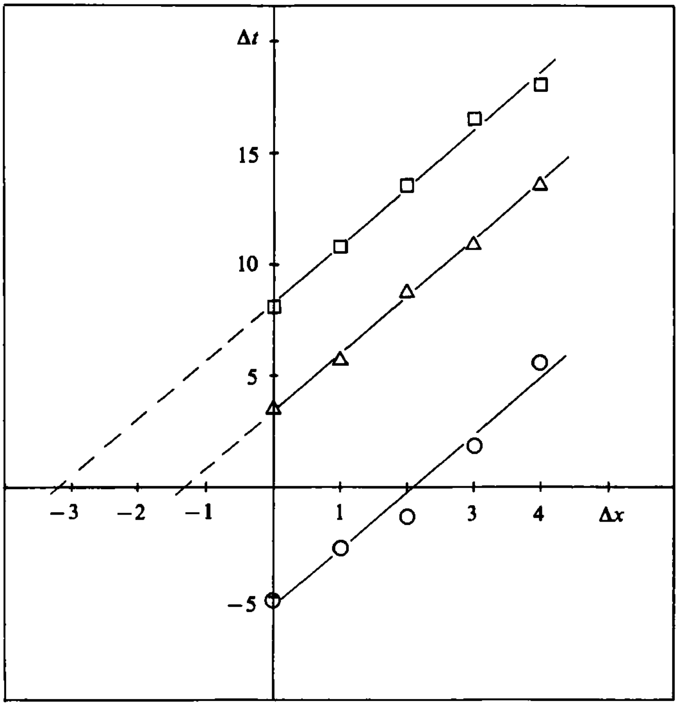

FIGURE 9. Time delay for wave packet as function of downstream separation. The reference probe is at $x = 400, z = 62$. ○, $\Delta z = -2$; △, $\Delta z = 2$; □, $\Delta z = 4$.

when measured normal to the wave fronts (not shown in the figure) than in the streamwise direction. These results will be further discussed in §4 in conjunction with the theoretically determined amplitude distributions.

The symmetry properties of the wave packet were investigated by the use of two probes. One probe (DISA R15) was positioned close to the lower wall while the other (TSI 1260-10W) was mounted on a three-degrees-of-freedom micrometer-controlled traversing mechanism, so that its sensor could be located close to the upper wall and above the sensor of the DISA-probe. Each probe was positioned at the y-locations where the wave amplitude was close to its maximum value, at the lower and upper walls, respectively. The high-pass-filtered anemometer voltage signals shown in figure 7 clearly show that the u-disturbance associated with the wave packet was antisymmetric. However, other disturbances were seen as well and these were symmetric. They occurred randomly in time, even when no spot was present, and their amplitude was much smaller than that of the wave packets of interest.

To characterize the wave packet we determined the angular frequency (ω), phase velocity in the streamwise direction (c), wavelength (or wavenumber ($k = (\alpha^2+\beta^2)^{\frac{1}{2}}$), where α and β are the wavenumbers in the streamwise and spanwise directions, respectively) and inclination (ϕ, defined as the angle between the streamwise direction and the wavenumber vector). For this two probes were used simultaneously, one probe was used as a reference at a fixed position, while the other was movable (see figure 8). Both probes were positioned close to the lower wall where the wave amplitude had its maximum and the time difference between the two signals was determined as a function of the downstream separation. Figure 9 shows the relation for three spanwise positions, where each point represents an average over three wave

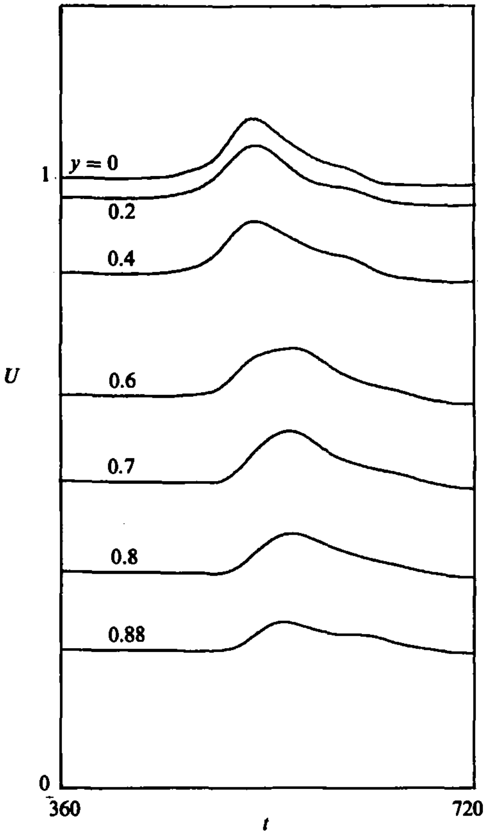

FIGURE 10. Ensemble-averaged, low-pass-filtered velocity signals outside the wingtip of the spot. $x = 400, z = 62$.

packets. There is a linear relation between the time difference and the downstream distance, and the slope of this line gives the phase velocity. The wavenumber in the streamwise direction was calculated as $\alpha = \omega/c$, and ω was obtained from the measured time separation of the first two maxima and minima of the signals. If the probes were positioned in such a way that the time difference was zero, then they would be aligned along the wave crests and the inclination angle could easily be determined. This position can be obtained by extrapolation from figure 9. The measured wave properties together with results from earlier visualization studies are shown in table 1.

3.3. *Velocity field outside the spot*

Outside the turbulent part of the spot both the streamwise and spanwise velocity components change (the latter is zero for the undisturbed flow). Typical ensemble averages of the low-pass-filtered streamwise velocity signals at seven different y-positions ($x = 400, z = 62$), where the average at each position consisted of ten different spots, are shown in figure 10. The triggering time was chosen as the reference time. The velocity profiles were obtained by fitting modified parabolas to these ensemble-averaged velocity measurements. The expression used for the velocity profiles was:

$$U(y,t) = (1-y^2)(C_0(t)+C_1(t)\,y^2+C_2(t)\,y^4), \tag{2}$$

x	$\phi(°)$	ω	c	k
160 (hot film)	64	0.44	0.53	1.89
400 (hot film)	40	0.40	0.38	1.37
400 (visual)	40	—	—	1.4

TABLE 1. Wave properties at $Re = 1500$

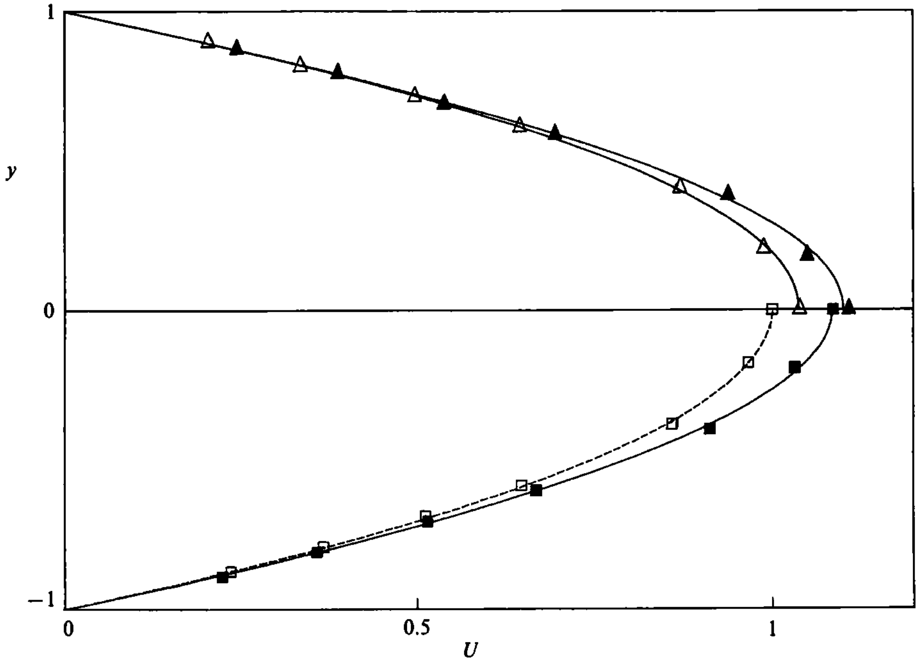

FIGURE 11. Measured and fitted streamwise mean velocity profiles at three different spanwise positions for $x = 400$. ----, parabolic profile; □, $z = 60$; ——, fitted profiles; ▲, $z = 60, t = 518$; ■, $z = 62, t = 518$; △, $z = 94, t = 518$.

where C_0, C_1, C_2 were determined by a least-squares fit. This gave a series of profiles each representing the velocity outside the spot at a specified time. Figure 11 shows the measured undisturbed profile which was found to be close to parabolic. Three measured profiles at $t = 518$ at various spanwise positions are also shown, together with the fitted profiles (equation (2)). One may note that the region of excess velocity has a fairly large extent in the spanwise direction.

Figure 12 shows ensemble-averaged W-profiles in the region where the waves are seen. The measurements were made with the technique described in §2. Downstream of the spot the flow direction was towards the symmetry plane over the whole channel width. When the wingtip has passed, the flow close to the wall was still in the same direction, whereas the flow in the centre of the channel was away from the spot.

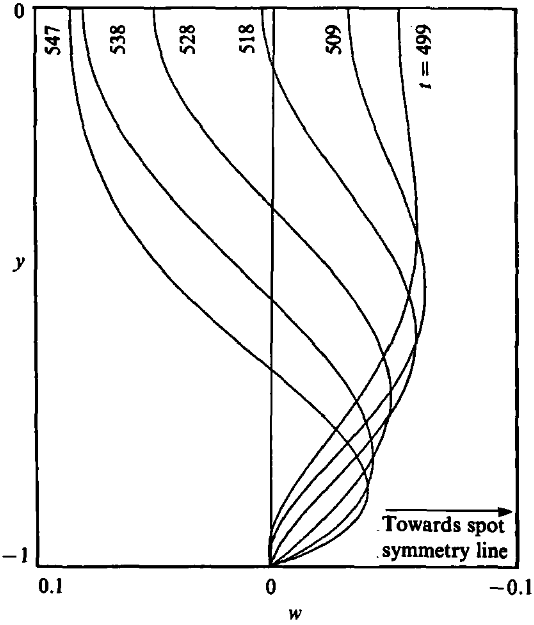

FIGURE 12. Spanwise velocity profiles at $x = 400, z = 62$.

4. Stability calculations

The laminar velocity field outside a turbulent spot is significantly altered by the presence of the spot. If the flow field is considered to be quasi-steady and quasi-homogeneous its stability properties can be analysed using the Orr–Sommerfeld equation. This assumption may be justified by noting that the wavelength is an order of magnitude smaller than the lengthscale of the mean flow variation (figure 4).

The main reason for carrying out stability calculations was to find out if the measured properties of the oblique waves at the wingtips could be reproduced by the linear stability theory. Oblique waves may be transformed with Squire's transformation to equivalent two-dimensional waves and compared with the solution to a two-dimensional Orr–Sommerfeld equation. By using an extended Squire's transformation one can not only transform oblique waves, but also waves superimposed on a mean velocity field having a spanwise component, to an equivalent two-dimensional problem (Landahl & Mollo-Christensen 1986 p. 93; see also Appendix). This is done by interchanging the usual $U(y)$ velocity in the Orr–Sommerfeld equation to the following expression:

$$U(y) + W(y) \tan\phi$$

where ϕ is the angle of the wavenumber vector to the streamwise direction. If the hot-film sensor is positioned normal to the wavenumber vector (i.e. $\psi = \phi$) it turns out that nominally this combination of the velocity components is measured (see equation (1)).

To get a measure of the departure of the fitted velocity profiles from the parabolic, the shape factor was calculated. The shape factor is the ratio between the displacement (δ_*) and the momentum-loss (θ) thicknesses, and may may be used as a measure of the fullness and hence the stability of the profile. The shape factor for the parabolic profile is 2.5 and the results from four measurements at $x = 400$ and

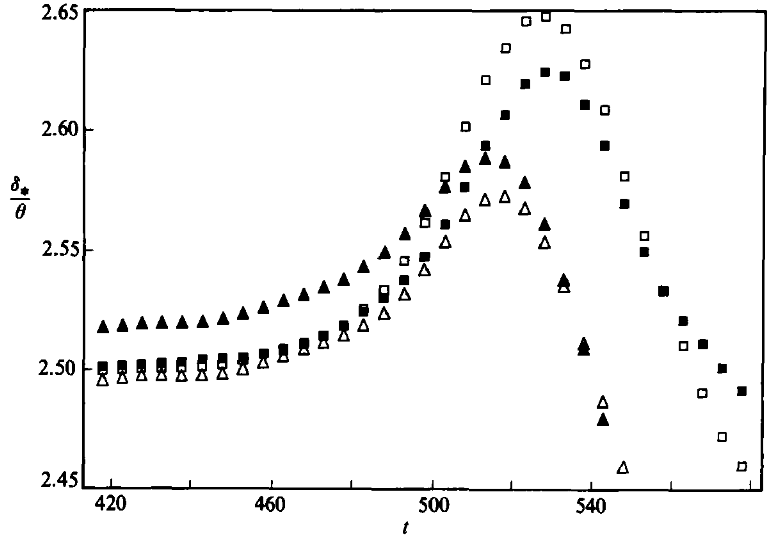

FIGURE 13. Shape-factor variation during spot passage at $x = 400, z = 62$. △, ▲, two independent U velocity measurement; □, ■, two independent $U + W\tan\phi$ velocity measurement.

$z = 62$ are shown in figure 13. The two that include the spanwise component have a maximum of a higher magnitude than those without, indicating that the spanwise component has a destabilizing effect. When the spanwise velocity is included the maximum occurs at a later time which corresponds to the time when the waves are first observed in the measurements.

4.1. *Eigenvalues and group velocities*

The Orr–Sommerfeld equation was solved to obtain the complex eigenvalues c, where the real part c_r is the phase velocity in the streamwise direction and the imaginary part c_i determines the growth or decay of the waves. It was solved with a shooting method using a fourth-order Runge–Kutta scheme. By orthonormalization of the eigenfunction (see Conte 1966) and stretching the y-coordinate close to the wall the accuracy of the solution was increased. The program was checked against known eigenvalues for the parabolic profile (Orszag 1971) and good agreement was obtained.

Calculations were made for measurements at both streamwise positions but only results from $x = 400$ will be presented here, since this was the only position where the spanwise component was measured. The eigenvalues c were calculated for the least damped symmetric mode for each series of profiles using the measured wave parameters ($k = 1.37, \phi = 40°$ and $Re = 1500$) as input. The absolute magnitude of the eigenvalues was sensitive to the variation of the fitted profiles, however, their qualitative variations were reproducible as they varied in time during the passage of the spot. The measured profiles had a somewhat higher value of c_r than the parabolic profile (table 2), but the variation was as large as $\pm 10\%$.

The variations of c_i at $x = 400$ and $z = 62$ during the spot passage are shown in figure 14. To be able to compare the qualitative features of c_i the departure from the parabolic case ($c_{i\text{par}} = -0.026$) is plotted with the maximum of each separate calculation series normalized to one. This way of plotting was chosen to show that the trends were reproducible even though the absolute magnitude of c_i varied. The destabilizing effect of the spot passage is clearly seen. Note the difference between the

	c_r	c_i	c_{gx}	c_{gz}	$\arctan(c_{gz}/c_{gx})$
U	0.42	−0.01	0.50	0.12	13°
$U+W\tan\phi$	0.42	0.01	0.55	0.12	12°
Parabola	0.39	−0.026	0.451	0.102	12.8°

TABLE 2. Typical calculated wave properties at $t = 518$ for $k = 1.37$, $\phi = 40°$, $Re = 1500$

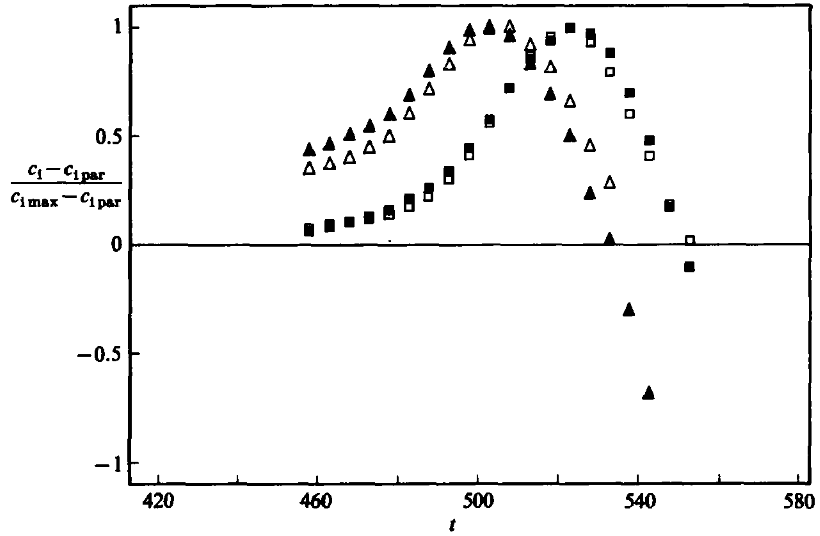

FIGURE 14. Instability parameter for four measured velocity profiles at $x = 400, z = 62$. For symbols, see figure 13.

calculations with only the streamwise component and those where the velocity profile included the spanwise component. The difference is consistent with the variation of the shape factor (figure 13) showing that the most unstable waves are found at a later time when the spanwise velocity component is included in the mean velocity profile. The inclusion of the spanwise velocity actually made the waves unstable (i.e. $c_i > 0$), whereas they were always damped (i.e. $c_i < 0$) if the spanwise component was disregarded (see table 2).

The two components of the group velocity for the considered wavenumber can be obtained by calculating the derivatives of c with respect to the wavenumbers α and β, and using Squire's transformation. The result is:

$$c_{gx} = c_2 + \frac{\alpha_3^2}{k}\frac{\partial c_2}{\partial \alpha_2} + \frac{Re_3\,\alpha_3\,\beta_3^2}{k^3}\frac{\partial c_2}{\partial Re_2}, \quad c_{gz} = \frac{\alpha_3\beta_3}{k}\frac{\partial c_2}{\partial \alpha_2} - \frac{Re_3\,\alpha_3^2\,\beta_3}{k^3}\frac{\partial c_2}{\partial Re_2},$$

where the subscripts 2 and 3 refer to the two- and three-dimensional form of the Orr–Sommerfeld equation, respectively (see Appendix). When the group velocities were calculated the real parts of the eigenvalues were used. This can be justified if the imaginary part of the phase velocity is small and the propagation of the wave packet is considered only for small times (see Landahl 1982).

The calculations showed an increase of both the streamwise and spanwise components of the group velocity when the altered velocity profiles were used. The increase was largest when the spanwise velocity component was included in the mean velocity profile (table 2). However, the calculated group velocity was smaller than the measured wingtip velocity. The angle of the group velocity vector to the streamwise direction remained approximately the same at 12°–13°. This angle was a few degrees greater than the spreading angle of the spot at the corresponding Reynolds number.

4.2. *Eigenfunctions and amplitude variations*

The vertical amplitude variation of the streamwise velocity component of the wave disturbance may be found by first calculating the eigenfunction of the normal velocity, and then using it in a forcing term when solving for the streamwise velocity (see Appendix). The symmetry properties of the normal and streamwise disturbance velocity components are opposite (this can be found by examining the corresponding equations). The eigenvalues previously calculated were for the least damped symmetric mode, this means that the corresponding amplitude dependence for the streamwise disturbance velocity is antisymmetric, in agreement with the experiments (figure 7). The calculated streamwise amplitude dependence (using equation (A 1), at $x = 400, z = 62, t = 518$) showed good agreement with the measured wave amplitudes (see figure 6, the two curves represent two independent measurement series). The amplitude of the waves in the direction of the wavenumber vector was also calculated (see Appendix) and was found to be smaller than the streamwise amplitude, in agreement with experiments. This was anticipated since the change in the horizontal velocity resulting from the displacement of fluid elements normal to the wall by the wave is proportional to the normal gradient of the mean flow in the direction considered. In this case the gradient of the streamwise component is much larger than that of the spanwise.

5. Discussion and conclusions

Boundary-layer spots have a spreading half-angle of typically 10° independent of the Reynolds number (Wygnanski, Zilberman & Haritonidis 1982), whereas the spreading rate of turbulent spots in plane Poiseuille flow increases nearly linearly with Reynolds number. For large (but still subcritical) Reynolds numbers it is substantially higher in plane Poiseuille flow. This may indicate that the spreading mechanism is different for the two cases, and that the observed wave packets play an important role in the spreading in the case of plane Poiseuille flow. The properties of these waves were compared to those calculated using the Orr–Sommerfeld equation with the measured velocity profiles and wavenumber vector of the observed waves as input. The phase speeds agreed approximately, the symmetry properties were correct, i.e. the u-disturbance was antisymmetric which implies symmetry in v, and the calculated y-dependence of the streamwise velocity disturbance was in fair agreement with the measured data. These results indicate that the assumptions of a quasi-steady and quasi-homogeneous mean flow field is justified, and the conclusion may be drawn that the observed wave packet consisted of the least damped symmetric T–S eigenmode.

The profiles of the spanwise velocity shows a velocity towards the spot downstream and a velocity away from the spot upstream of the wingtip. This is consistent with the idea of Widnall (1984) that the spot may be considered as an area of partial flow blockage. One may also note however, that the spanwise velocity close to the wall always seems to be directed into the spot.

The possibility of directly measuring the required mean velocity profile in the generalized Orr–Sommerfeld equation is demonstrated in the present paper. This results in good accuracy since there is no need to obtain the spanwise velocity explicitly as a difference of two measured signals, and since only one sensor is needed good spatial resolution is obtained. When the spanwise component was taken into account the calculated growth rate became positive with its maximum found at the time when the waves were observed.

In previous work (see e.g. Gad-el-Hak, Blackwelder & Riley 1981) a possible explanation for the rapid spanwise growth of a turbulent spot has been 'growth by destabilization'. Our calculations did indeed indicate that the flow outside a spot was less stable than the undisturbed laminar flow. However, the calculated growth factor of 0.01 is too small in itself to explain breakdown, since it would take about 15 channel heights for the waves to double in amplitude.

Another possible mechanism for the build-up of the rather large wave amplitudes may be the wave trapping mechanism proposed by Landahl (1972). He used it to explain the transition process in a boundary layer disturbed by a vibrating ribbon and found that when the group velocity of a small scale (secondary) disturbance is equal to the phase velocity of a large scale (primary) disturbance the wave energy is trapped and breakdown occurs. In our measurements a similar situation existed, where the wave packet coincided with a large-scale velocity disturbance. This region of excess velocity outside the wingtip could be considered as the primary wave and the smaller scale T–S waves as the secondary waves. The calculated group velocity of the T–S waves increased (from about 0.45 to around 0.55) when the altered velocity field was used in the Orr–Sommerfeld calculation, but it was always smaller than the propagation velocity of the area of excess velocity where the waves were observed (about 0.75).

Once the T–S waves have acquired their rather large amplitude they may become unstable to smaller scale three-dimensional disturbances, which may result in breakdown. This route to transition has been observed both experimentally (Klebanoff *et al.* 1961; Nishioka *et al.* 1975) and theoretically (Orszag & Patera 1983).

Finally, it is not yet clear how or why the specific waves observed were singled out from all the possible solutions to the Orr–Sommerfeld equation. Widnall (1984) calculated the far-field wave pattern from a moving point disturbance. She assumed the wave pattern to be stationary in the frame of reference of the disturbance. The wave pattern in the wingtip area was in qualitative agreement with spot flow visualization. The present work showed, however, that the wave crests are not stationary with respect to the spot, their phase velocity was around 0.4 which is much smaller than the celerity of the wingtip (0.75).

The present study was supported by STU, the Swedish Board for Technical Development.

Appendix

An extended form of the Orr–Sommerfeld equation can be obtained by linearizing the Navier–Stokes equations around a mean flow of the form $(U_3(y), 0, W(y))$ and separating the disturbance variables into Fourier components e.g. $v_3(x,y,z,t) = \hat{v}_3(y;\alpha_3,\beta_3,c_3)\exp\{\mathrm{i}(x\alpha_3+z\beta_3-\alpha_3 c_3 t)\}$, the subscript 3 indicates that we are considering the three-dimensional version of the Orr–Sommerfeld equation).

After the pressure is eliminated the following equation for the Fourier components for the normal disturbance velocity can be obtained:

$$(U_3+W\tan\phi-c_3)(\mathrm{d}^2/\mathrm{d}y^2-k^2)\,\hat{v}_3-(U_3''+W''\tan\phi)\,\hat{v}_3-\frac{(\mathrm{d}^2/\mathrm{d}y^2-k^2)^2\,\hat{v}_3}{\mathrm{i}\alpha_3 Re_3}=0.$$

The two-dimensional version reads as follows:

$$(U_2-c_2)(\mathrm{d}^2/\mathrm{d}y^2-\alpha_2^2)\,\hat{v}_2-U_2''\,\hat{v}_2-\frac{(\mathrm{d}^2/\mathrm{d}y^2-\alpha_2^2)^2\,\hat{v}_2}{\mathrm{i}\alpha_2 Re_2}=0,$$

where the subscript 2 refers to the two-dimensionality. The eigenvalue problems are seen to be equivalent if the following holds

$$c_2=c_3,\quad \alpha_2=k,\quad Re_2=Re_3\cos\phi,\quad U_2=U_3+W\tan\phi,$$

where we have used $\alpha_3=k\cos\phi$. This is, in fact, an extended form of Squire's transformation (see Landahl & Mollo-Christensen 1986 p. 93).

An equation for the Fourier components $\hat{u}_3$ and $\hat{w}_3$ of the streamwise and spanwise disturbance velocities, respectively, can be obtained in a manner similar to that in which the Orr–Sommerfeld equation is derived:

$$A\hat{u}_3=-\hat{v}_3\,U_3'-\mathrm{i}\alpha_3\,\hat{p}_3, \tag{A 1}$$

$$A\hat{w}_3=-\hat{v}_3\,W'-\mathrm{i}\beta_3\,\hat{p}_3, \tag{A 2}$$

where the operator A is defined as follows

$$A=\mathrm{i}\alpha_3(U_3+W\tan\phi-c_3)-\frac{(\mathrm{d}^2/\mathrm{d}y^2-k^2)}{Re_3},$$

and

$$\hat{p}_3=\frac{(-A\hat{v}_3'+\mathrm{i}\alpha_3\,\hat{v}_3(U_3'+W'\tan\phi))}{k^2}.$$

By first solving the Orr–Sommerfeld equation to obtain $\hat{v}_3$ and using that solution in (A 1) it is possible to determine $\hat{u}_3$. One may note that if $\hat{v}_3$ is symmetric $\hat{u}_3$ will be antisymmetric since the forcing will have the opposite symmetry properties of $\hat{v}_3$. Note also that if the wave amplitude in the direction of the wavenumber vector $((\alpha_3\,\hat{u}_3+\beta_3\,\hat{w}_3)/k)$ is desired the resulting combination of (A 1) and (A 2) will become the continuity equation.

REFERENCES

Alavyoon, F., Henningson, D. S. & Alfredsson, P. H. 1986 Turbulent spots in plane Poiseuille flow – flow visualization. *Phys. Fluids* **29**, 1328.

Carlson, D. R., Widnall, S. E. & Peeters, M. F. 1982 A flow-visualization study of spots in plane Poiseuille flow. *J. Fluid Mech.* **121**, 487.

Chambers, F. W. & Thomas, A. S. W. 1983 Turbulent spots, wave packets, and growth. *Phys. Fluids* **26**, 1160.

Conte, S. D. 1966 The numerical solution of linear boundary value problems. *SIAM Rev.* **8**, 309.

Gad-el-Hak, M., Blackwelder, R. F. & Riley, J. J. 1981 On the growth of turbulent regions in laminar boundary layers. *J. Fluid Mech.* **110**, 73.

Gaster, M. 1975 A theoretical model of a wave packet in the boundary layer on a flat plate. *Proc. R. Soc. Lond* A **347**, 271.

Gaster, M. & Grant, I. 1975 An experimental investigation of the formation and development of a wave packet in a laminar boundary layer. *Proc. R. Soc. Lond.* A **347**, 253.

KLEBANOFF, P. S., TIDSTROM, K. D. & SARGENT, L. M. 1961 The three-dimensional nature of boundary layer instability. *J. Fluid Mech.* **12**, 1.

LANDAHL, M. T. 1972 Wave mechanics of breakdown. *J. Fluid Mech.* **56**, 775.

LANDAHL, M. T. 1982 The application of kinematic wave theory to wave trains and packets with small dissipation. *Phys. Fluids* **25**, 1512.

LANDAHL, M. T. & MOLLO-CHRISTENSEN, E. 1986 *Turbulence and Random Phenomena in Fluid Mechanics*. Cambridge University Press.

NISHIOKA, M., IIDA, S. & ICHIKAWA, Y. 1975 An experimental investigation of the stability of plane Poiseuille flow. *J. Fluid Mech.* **72**, 731.

ORSZAG, S. A. 1971 Accurate solution of the Orr–Sommerfeld stability equation. *J. Fluid Mech.* **50**, 689.

ORSZAG, S. A. & PATERA, A. T. 1983 Secondary instability of wall bounded shear flows. *J. Fluid Mech.* **128**, 347.

WIDNALL, S. E. 1984 Growth of turbulent spots in plane Poiseuille flow. In *Turbulence and chaotic phenomena in fluids* (ed. T. Tatsumi), p. 93. Elsevier.

WYGNANSKI, I., HARITONIDIS, J. H. & KAPLAN, R. E. 1979 On a Tollmien–Schlichting wave packet produced by a turbulent spot. *J. Fluid Mech.* **92**, 505.

WYGNANSKI, I., ZILBERMAN, M. & HARITONIDIS, J. H. 1982 On the spreading of a turbulent spot in the absence of a pressure gradient. *J. Fluid Mech.* **123**, 69.